Organic Crystal Packing is Key to Determining Photomechanical Response

Cameron J. Cook, Cody J. Perry, and Gregory J. O. Beran*

Department of Chemistry, University of California, Riverside, California 92521 USA

E-mail: gregory.beran@ucr.edu

Abstract

Organic photomechanical crystals have great promise as molecular machines, but their development has been hindered by the lack of clear theoretical design principles. While much research has focused on the choice of the molecular photochrome, density functional theory calculations here demonstrate that crystal packing has a major impact on the work densities that can be produced by a photochrome. Examination of two diarylethene molecules reveals that the predicted work densities can vary by an order of magnitude across different experimentally-known crystal structures of the same species. The largest work densities occur when molecules are aligned in parallel, thereby producing a highly anisotropic photomechanical response. These results suggest that a greater emphasis on polymorph screening and/or crystal engineering could improve the work densities achieved by photomechanical engines. Finally, an inherent thermodynamic asymmetry is identified that biases photomechanical engines to exhibit larger work densities in the forward stroke direction.

TOC Graphic

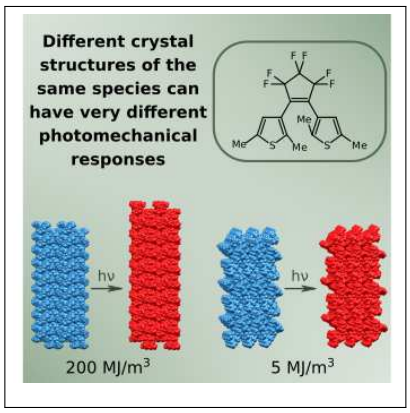

Artificial molecular machines exploit chemical, electronic, or photonic inputs to perform nanoscale to macroscopic work.[1–5] Photomechanical molecular crystals are a promising class of machine which converts light into mechanical motion via photochemically-induced structural changes.[6–10] Photomechanical molecular crystals offer many advantages: Their unique combination of high elastic modulus and high strain[11–13] leads to elastic work densities which are potentially several orders of magnitude larger than piezoelectric actuators or elastomers. Organic crystal work outputs per unit of mass are even more impressive than the volumetric ones, especially when compared to inorganic materials. Light-driven actuators can be controlled with high-precision by varying the position, frequency, intensity, and polarization of light, all without physical contact or the need for secondary chemical fuels. Furthermore, the infinite chemical tunability of photochromes promises the ability to engineer specific properties into the material.

Many photochromes have been studied to-date,[7,8,10] including cis-trans isomerization of azobenzene derivatives[14] and salicylideneanilines,[15,16] ring-opening and closing of diarylethenes,[17–26] and various [2+2][27–30] and [4+4][31–34] photodimerization reactions. Photomechanical responses have been exploited to produce organic crystal cantilevers that can lift objects several orders of magnitude heavier,[17,20,35,36] to induce locomotion[37] and flagellar motion,[38] and even to create waveguides.[39,40] Several reviews discuss the general mechanisms underlying these photomechanical responses.[6,7,9]

While the molecular tunability of diarylethenes and other photochromes has been explored frequently, fewer studies have investigated the impact of crystal packing on the photomechanical responses. Experimental studies demonstrate that polymorphism[16,25,41–44] and variations in crystal packing across closely-related molecules[44,45] can significantly alter the photomechanical response properties. Unfortunately, a thorough understanding that bridges between molecular structure, crystal structure, and photomechanical response remains elusive. Moreover, the potential search space of photochromic molecules and crystals is massive. Accelerating the discovery of useful new photomechanical materials requires establishing crystalline design principles that lead to high performance, thereby reducing the need for time-consuming trial-and-error experimental testing.

For these reasons, we recently developed a theoretical framework for modeling photomechanical crystal engines from first principles.[46] Starting from either the experimental or predicted crystal structure of the reactant, the topochemical crystal-to-crystal phototransformation to the product is predicted using density functional theory (DFT). An idealized thermodynamic engine cycle is then employed to compute the maximum work that could potentially be performed by that structural transformation. This approach successfully predicts the experimental photochemical transformations for multiple anthracene [4+4] photodimerization systems.[46]

In the present study, we elucidate new molecular crystal design principles for photomechanical actuators by applying these same modeling techniques to multiple crystal forms of diarylethenes **1**[41] and **2**[47–49] (Figure 1). We demonstrate how control over crystal packing is key for achieving large photomechanical responses and high work densities: the range of work densities observed across different experimental crystal structures of the same species greatly exceeds the variations found between different photochromic reactions. This highlights the central importance of polymorph screening and crystal engineering for designing high-performance photomechanical materials. By investigating how unit cells deform from reactant to product and the associated stresses, we identify key crystal packing features that generate large work densities. Finally, an inherent thermodynamic asymmetry is identified which biases photomechanical molecular crystal engines to produce more work on the forward stroke than the reverse one, implying that the ability to perform net work is a general feature of these crystal engines. Together, these theoretical insights provide a road

map for the future experimental realization of better-performing photomechanical engines.

Diarylethenes are probably the best-studied photochrome, and they offer many advantages as photomechanical materials: strong thermal stability, fast picosecond reactivity and microsecond deformation of the crystal,[17,20] high quantum yields for ring closing, and excellent fatigue resistance over thousands of cycles.[26] The relatively small changes in molecular shape upon ring-opening and closing enables bulk crystals to react without shattering. In addition to their highly tunable photochromism,[26,50,51] diarylethene crystals can undergo photomechanical twisting, rolling, bending, swinging, and jumping (salience).[18,19,22–25] On the other hand, the work output is limited in practice by the difficulty in reacting more than ∼5–15% of the molecules in the crystal experimentally,[21,25,48,49,52] due to factors such as the limited light penetration into the crystal and the photostationary state established due to the overlapping absorption bands of the reactant and product forms.[6]

Let us consider the diarylethene species shown in Figure 1. **1a** has four reported crystal polymorphs (α, β, γ, and δ).[41] All four exhibit suitable anti-parallel orientations[53] of the central methyl groups to undergo solid-state photochromic ring closing upon 370 nm irradiation, and the reaction can be reversed with visible light >500 nm. The crystal structures formed via the solid-state reaction of **1a**-α,β,γ,δ have not been determined experimentally. One solid form of **1b** crystallized from solution has also been characterized,[41] though its solid-state reactivity has not been reported. We also examine open (**2a**) and closed (**2b**) forms of **2**, whose solid-state transformations have been better characterized experimentally. As noted earlier, achieving complete photochemical conversion of diarylethene crystals is experimentally difficult, but partially photo-reacted crystals of **2a** and **2b** have been solved as a mixture of open- and closed-form components (Cambridge Structure Database Reference Codes FAWFOY02 and FAWFOY01, respectively).[48,49]

To understand how crystal packing impacts the photomechanical response in these seven crystals, we begin by predicting the unknown solid-state photochemical crystal transformations using the crystalline topochemical approach we recently applied[46] to the solid-state photodimerization of 9-methyl anthracene (9MA),[54,55] 9-tert-butyl anthracene ester (9TBAE),[31,56,57] and monoclinic 9-anthracene carboxylic acid (9AC).[32,58] That study replaced pairs of anthracene molecules from the reactant crystals with their photodimer products positioned to minimize the molecular translation and rotation (by maintaining the center of mass and aligning the axes of inertia). The structures obtained after subsequent DFT optimization of these topochemically-generated product crystals closely match the experimental photodimer crystal structures.[46] Conceptually similar approaches have been used to help interpret experiments on **2**[47–49] and in a few other systems.[59,60]

Here, we apply the same principles to predict the transformations for the seven experimental crystal forms of **1** and **2**, using planewave DFT under periodic boundary conditions[61] with the B86bPBE density functional[62,63] and the exchange hole dipole moment (XDM) dispersion correction.[64] We focus first on the experimentally-reported, partially reacted crystal structure of **2a** (FAWFOY02), which contains 92% open-form (reactant) and 8% closed-form (product) molecules. To predict the product topochemically, we take the experimental atomic coordinates of the open-form **2a** species from FAWFOY02, replace them with closed-form **2b** molecules at the same positions and orientations, and then perform an unconstrained DFT relaxation on the resulting unit cell. This topochemically-predicted product almost perfectly matches the crystal structure obtained by instead optimizing the experimental closed-form **2b** product component of FAWFOY02 with DFT (15-molecule root-mean-square deviation,[65] rmsd15 = 0.13 Å, Figure S1).

Similarly, applying the same procedure to partially reacted crystals of **2b** (FAWFOY01), taking the closed-form coordinates, converting the molecules to their open form, and relaxing gives a structure that matches

the open form from the partially-reacted crystals of **2b** (rmsd15 = 0.28 Å, Figure S1). The excellent agreement between the topochemically-generated product crystals and the experimentally-determined photochemical product structures for diarylethenes **2a**/**2b** and the earlier anthracenes[46] validates the topochemical approach used here. As was seen for the anthracenes[46,56,66] and in earlier experiments on **2**,[67] the solid-state photochemical reactions generate product crystal structures which retain the qualitative packing motifs of their respective reactant crystals (Figure 2). They differ from the polymorphs obtained by crystallizing the product molecule from solution.

Having demonstrated that the solid-state photochemical transformations of diarylethene **2** can be predicted *in silico*, the same procedure is employed to predict the transformations of the five crystal structures of **1a** and **1b** (Figure 2). The ring-closing reaction of **1a** generally increases the planarity of the molecular backbone, including the dihedral angles relating the thiophene and phenyl rings. However, the impact of the photochromic reaction on the crystal unit cells varies widely across the different crystal forms. For example, ring-closing increases the predicted molar volume for **1a-**β (+6.1%), **1a-**γ (+4.6%), **1a-**δ (+3.3%), while it decreases it for **1a-**α (-1.8%) and **1b** (-2.0%). The individual lattice parameter changes also vary considerably across different polymorphs. **1a-**β shows the largest volume change, and it exhibits the most isotropic lattice parameter changes. In contrast, the transformations in the other forms of **1** are more anisotropic, with e.g. significant elongation/contraction along the a and b axes of **1b** and **1a-**γ or a large contraction of the β angle in **1a-**δ. The most substantial transformation occurs for the **1a-**α polymorph, which deforms from a monoclinic to a triclinic cell with large changes in both the lattice constants and angles.

The contrast between the transformations of solid-state **2a** and **2b** is even larger: whereas the ring-opening of **2b** alters its lattice parameters by ∼2% or less, ring-closing of **2a** expands along b by 17.4% while simultaneously contracting 8.4% along a. This would represent an unusually large dimensional change for photomechanical crystal, though it is still considerably smaller than the ∼40-50% expansions reported experimentally for two other organic crystal transformations.[68,69]

To understand how these crystal structure changes translate to the amount of work that could hypothetically be performed via linear actuation, we model these systems as an idealized photomechanical engine (Figure 3).[46] Inspired by traditional gas heat engines, this photomechanical engine cycle involves four steps: (1) fast, complete solid-state photochemical conversion of the reactant to produce the "proto-product" crystal (i.e. product molecules constrained within the lattice parameters of the reactant), (2) structural relaxation of the proto-product structure to the equilibrium product crystal structure, (3) fast, complete solid-state conversion of the product back to the "proto-reactant" crystal (reactant molecules within the product lattice parameters), and (4) structural relaxation of the proto-reactant back to the original reactant crystal structure.

The "proto-" structures generated by Steps 1 and 3 are obtained by relaxing the topochemically-seeded product molecules within the fixed unit cell parameters of the reactant crystals. These strained "proto-" structures exhibit internal stress. The subsequent DFT relaxation of the lattice parameters and atomic coordinates relieves that stress and strain by deforming the crystal, thereby performing elastic work in the "forward" (Step 2) or "reverse" (Step 4) directions. The assumption of a fast, complete reaction without lattice relaxation in Steps 1 & 3 maximizes the stress created and establishes an upper bound to the potential work that could be performed. In practice, incomplete reaction frequently leads to the formation of bimorph structures and bending,[6,7,9] which results in lower work densities.[12] Even if the ideal work densities predicted are not achieved experimentally, this theoretical photomechanical engine scheme provides valuable insights into the relationships between crystal packing and work density, as will be discussed below. Additional discussion of the

idealized photomechanical engine cycle can be found in Ref 46.

Figure 4 summarizes the energies for the engine cycles of each species. Given the potential impacts of intramolecular DFT delocalization error on photochromic reactions[45,66] and other processes[70–77] that alter the extent of π conjugation, these energies were computed via a hybrid approach[74] that combines a domain-local pair natural orbital coupled cluster singles and doubles plus perturbative triples (DLPNO-CCSD(T1))[78,79] description of the intramolecular energy with the B86bPBE-XDM DFT treatment of the intermolecular interactions (SI Section S1.2). From the DFT-computed stress (σ) and strain (ϵ) tensors for the "proto-" structure relative to the relaxed one, the anisotropic elastic work is computed (SI Section S1.4) over a set of unit vectors $\hat{n}$ spanning all crystallographic directions,

$$W(\hat{n}) = -\frac{1}{2}\hat{n}^{\intercal}\sigma\epsilon\hat{n} \quad (1)$$

The resulting work densities are plotted as a heat map on the surface of a sphere (Figure 5) that highlights the crystallographic directions along which significant work is performed. Table 1 summarizes the maximum value of the work density obtained for each solid-state reaction after scanning over all crystallographic directions. Within the idealized engine model, these maximal values represent the most work a linear actuator could achieve, assuming fast, complete photochemical conversion and suitable crystal orientation/device morphology.

These theoretical engine cycles reveal several interesting features to guide the design of new photomechanical materials. Similar to what has been found previously in anthracene photodimerization systems,[46,66] the polymorphs produced by the solid-state photochemical reactions are thermodynamically unstable, lying 13–33 kJ/mol above the most stable polymorphs crystallized from solution. Such high-energy polymorphs would almost certainly be inaccessible via traditional crystallization, since the vast majority of experimentally-observed molecular crystal polymorphs lie within 10 kJ/mol of the most stable structure.[80,81]

The predicted energy changes for each step also vary substantially across the different crystal forms of the same species (Figure 4). Large Step 2 & 4 relaxation energies occur for the crystals with large, anisotropic lattice parameter changes. For example, the large and highly anisotropic structure deformations upon ring-closing of **1a-**α and **2a** relax ∼40 kJ/mol, compared to only ∼10 kJ/mol or less for the smaller, more isotropic structure changes that occur in **1a-**β or **2b**. Because these energy changes relate to the total work done by the system upon the structure relaxation, we observe that **1a-**α converts 13% of an input 370 nm photon (323 kJ/mol) to forward (ring-closing) work, for example.

Table 1: Maximum predicted work densities (MJ/m^3) for each crystal system in the forward and reverse reaction directions.

Crystal	Forward	Reverse
	Ring-Closing	Ring-Opening
1a-α	104	83
1a-β	17	13
1a-γ	51	16
1a-δ	73	20
2a	200	40
	Ring-Opening	Ring-Closing
1b	46	12
2b	5	5
	Dimerization	Dissociation
9MA[a]	25	12
9AC mono.[a]	30	18
9TBAE[a]	47	16

[a] Results for anthracene photodimerization systems from Ref 46 included for comparison.

For actuation, however, it is interesting to examine the maximum work density that can performed along a particular crystallographic direction. As shown in Table 1, the maximum work density varies substantially across the different polymorphs. The maximum work densities are generally strongly aligned along a particular crystallographic direction (Figure 5), as will be discussed in more detail below. The

ring-closing of Form **1a-**α can theoretically produce up to 99 MJ/m^3 in one crystallographic direction, which is six times larger than the 17 MJ/m^3 maximum produced by the closing of **1a-**β. The maximum work densities of the other crystal forms of **1** lie between these extremes. The 200 MJ/m^3 maximum ring-closing work density of **2a** is even more exceptional. It is 40-times larger than the maximal work produced by the ring-opening of **2b**, and 4–8 times larger than the maximum predicted work densities for the solid-state [4+4] photodimerization reactions of 9MA, monoclinic 9AC, and 9TBAE (Table 1).[46] On the other hand, the diarylethene crystals with the smallest forward-direction work densities here (5–17 MJ/m^3 for **1a-**β and **2b**) produce only a fraction of the work densities generated by the anthracene photodimerizations. In other words, the range of work densities produced by different crystal polymorphs of a particular diarylethene molecule can be broader than the differences between the diarylethene opening/closing and anthracene [4+4] photodimerization reactions.

Although the difficulty of reacting diarylethene crystals completely and other practical limitations will hinder experimental realization of the ideal $\sim$10^7–10^8 J/m^3 theoretical work densities predicted here, the theoretical potential for such large work densities should motivate efforts further to measure and improve the experimental work densities of experimental photomechanical crystals. For context, previously reported experimentally work densities for thermosalient and photomechanical organic crystal actuators ($\sim$10–10^5 J/m^3),[11,12,68] photomechanical polymers (up to $\sim$10^5 J/m^3),[12,82] or piezoelectrics ($\sim$10^3 J/m^3)[11] are several orders of magnitude smaller, even if the aforementioned caveats regarding the predicted values noted above prevent direct comparison between the theoretical and experimental work densities. See Ref 68 for a summary of experimental work densities across many different materials.

More importantly, the order-of-magnitude variations in the predicted work densities across different diarylethene crystal forms clearly highlight the central role crystal packing plays in determining the photomechanical response properties. Closer examination of the structures reveals important design features underlying the large photomechanical responses. The largest work densities are produced by the crystals with parallel alignments of the reacting molecules (**1a-**α, **2a**). Such arrangements concentrate the photomechanical response along a single crystallographic direction (Figure 2), resulting in large anisotropic structural changes that produce substantial stress, lattice deformations, and work densities. In contrast, the low-work forms **1a-**β, **1b**, and **2b** pack molecules with multiple different orientations in the crystals, thereby producing more isotropic structural responses and much lower work densities.

For further insight, the correlation between the single largest-magnitude principal components of the stress and strain tensors versus the maximum work density were investigated (SI Section S3). Although work results from the product of both stress (force) and strain (displacement), the stress tensor components correlate more strongly ($R^2 = 0.89$) with the maximum work than do the strain tensor ones ($R^2 = 0.43$). This behavior can be understood in terms of the molecular nature of the materials. The largest work density typically occurs along the short axis of the diarylethene molecules (i.e. along the vertical axis for the molecules as drawn in Figure 1), as closing the ring necessitates increasing the intermolecular spacing in this direction. For **2a** or **1a-**γ, for example, the greatest work density lies along the b direction, which aligns with this short molecular axis (Figure 5a,c)). Even in **1a-**α, where the largest lattice parameter change occurs along the a axis (largely out of the plane of the molecule), the stress along the short molecular axis is larger and leads to more work along a direction in between b and c (Figure 5b). This is similar to 9TBAE, where the largest lattice parameter change after photodimerization involves the contraction of newly created void space along the b axis, but the expansion along a forced by the buckling of the anthracene rings produces more work.[46] In other words, large crystal deformations are an important but insufficient predictor of high work density. The

stress created by the solid-state reaction provides a better descriptor of which large deformations will manifest in high work densities.

The importance of stress over strain further manifests in the fact that the forward reactions in Table 1 generally produce considerably more work than the reverse ones, despite involving equal but opposite changes in the lattice parameters (i.e. comparable strains). Only **2b** is somewhat of an exception, with small 5 MJ/m^3 work magnitudes produced in both directions due to the minimal stress and lattice deformation induced by the photochemical reaction. The bias toward a larger forward work implies an inherent asymmetry in the stress between the forward versus reverse reactions. In our earlier anthracene [4+4] photodimerization study,[46] the larger forward work densities were attributed to the greater facility with which crystals comprised of planar anthracene monomers deform compared to those containing the bulkier photodimers. However that explanation is clearly insufficient, since the maximal work achieved for the diarylethenes is independent of the molecular structure: **1a** and **2a** show higher work density for ring-closing, but **1b** does so for the ring-opening.

Instead, the origin of this asymmetry lies in the fact that the initial crystal packing is determined by the reactant species. Even when the solid-state photochemical reaction generates product molecules, the crystal structure retains "memory" of the reactant crystal packing. This non-optimal packing of the product species places it on a steep and unstable region of the potential energy surface, as evidenced by the high polymorph energies of the product crystal noted earlier and the large Step 2 relaxation energies (Figure 4). In contrast, the reverse reaction generates the reactant in a crystal packing that is only modestly deformed from its original stable form. This corresponds to a flatter, more stable region of the reactant potential energy curve, as evidenced by the smaller Step 4 relaxation energies. Overall, this inherent thermodynamic bias of the engine toward the preferred crystal packing of the reactant molecule creates the asymmetry between the forward and reverse engine strokes that enables photomechanical engines to produce net work in the forward direction (almost) regardless of the specific chemistry.

In summary, this study has established several important structural design principles for high-work density photomechanical engines. For a given photochrome, crystal packing and polymorphism can alter the work density by an order of magnitude, demonstrating that future research ought to emphasize the design and control of solid-state structures in addition to the molecular chemistry. Crystal structures should align the molecules in a parallel fashion to maximize the anisotropic photomechanical response along a single crystallographic direction. While large structural deformations are helpful, the creation of high stress along those deformation modes is even more important to achieving high work densities. The calculations also reveal a relationship between molecular structure and the solid-state response: for the cases with well-aligned diarylethenes studied here, the maximum work density occurs primarily along the short axis of the diarylethene molecule. Finally, photomechanical engines have an inherent thermodynamic asymmetry arising from retained memory of the reactant crystal structure which biases them to perform more work in the forward stroke direction, independent of the specific photochrome.

The theoretical calculations also find that diarlyethenes can theoretically produce massive work densities of at least ∼100–200 MJ/m^3. The combination of these results and the ∼25–50 MJ/m^3 work densities previously predicted for several anthracene photodimerization systems[46] demonstrate the exceptional photomechanical properties of organic crystals. Achieving such work densities in real-world actuators faces serious experimental challenges, such as the need to react the molecules quickly to maximize the stress, to react them completely to achieve linear actuation (instead of bending), and to develop device architectures that can harness the work effectively. Nevertheless, an experimental actuator achieving even a fraction of these work densities could substantially outperform present-day devices.

Computational Methods

Experimental crystal structures were obtained from Cambridge Structure Database and both the lattice parameters and atomic positions were fully relaxed with periodic DFT. The initial topochemically-reacted structures were generated by replacing each unreacted molecules in the crystal with its reacted counterparts, maintaining the same center of mass and maximally aligning the product molecule's axes of inertia with the original reactant ones. The proto-product structure was then determined by DFT-optimizing this initial topochemically-generated structure with the lattice parameters frozen at their reactant crystal values. The final equilibrium product crystal was obtained via unconstrained variable-cell DFT relaxation of the topochemical product structure. The DFT-computed stress and strain tensors associated with the proto-product were used to compute the elastic work according to Eq 1.

All periodic DFT crystal calculations employed the dispersion-corrected B86bPBE-XDM functional in Quantum Espresso v6.7,[61] using a 50 Ry planewave cutoff and Monkhorst-Pack reciprocal space k-point densities of at least 0.05 $Å^{-1}$. The core electrons were treated in the projector augmented wave (PAW) approach using potentials generated with Atomic v6.1. To minimize potential density-driven delocalization error issues in the DFT reaction energies stemming from the change in π conjugation between the open and closed molecule forms, all final periodic DFT energies were adjusted with a single-point intramolecular energy correction. The correction was computed as the difference between the B86bPBE-XDM and domain-local pair natural orbital coupled cluster singles and doubles with perturbative triples (DLPNO-CCSD(T1))[78] intramolecular energies according to ref 74. The coupled cluster results were extrapolated to the complete-basis-set (CBS) limit by combining DLPNO-CCSD(T1)/aug-cc-pVDZ and CBS-limit second-order Møller-Plesset perturbation theory (MP2) results in a focal point approach. The MP2/CBS calculations were extrapolated from the aug-cc-pVTZ and aug-cc-pVQZ basis sets.[83] All MP2 and coupled cluster calculations were performed with Orca 5.0.[79] Further details of the experimental crystal structures, the electronic structure calculations, the basis set extrapolation, the topochemical reaction procedure, and the calculation of the work density can be found in Section S1 of the Supporting Information.

Acknowledgments

G.J.O.B. acknowledges support from the National Science Foundation (CHE-1955554) and supercomputer time from ACCESS (CHE110064). We thank Prof. Christopher Bardeen for helpful discussions and his comments on the manuscript.

Conflict of Interest

The authors declare no conflicts of interest.

Supporting Information

- Additional computational and methodological details.
- All DFT-computed crystal structures and analysis.
- Predicted stress & strain tensors, work density plots for all systems studied here, and analysis.

The Supporting Information is available free of charge at....

References

(1) Erbas-Cakmak, S.; Leigh, D. A.; McTernan, C. T.; Nussbaumer, A. L. Artificial Molecular Machines. *Chem. Rev.* **2015**, *115*, 10081–10206.

(2) Kassem, S.; van Leeuwen, T.; Lubbe, A. S.; Wilson, M. R.;

Feringa, B. L.; Leigh, D. A. Artificial Molecular Motors. *Chem. Soc. Rev.* **2017**, *46*, 2592–2621.

(3) Baroncini, M.; Casimiro, L.; de Vet, C.; Groppi, J.; Silvi, S.; Credi, A. Making and Operating Molecular Machines: A Multidisciplinary Challenge. *ChemistryOpen* **2018**, *7*, 169–179.

(4) Lancia, F.; Ryabchun, A.; Katsonis, N. Life-like Motion Driven by Artificial Molecular Machines. *Nature Rev. Chem.* **2019**, *3*, 536–551.

(5) Aprahamian, I. The Future of Molecular Machines. *ACS Cent. Sci.* **2020**, *6*, 347–358.

(6) Kim, T.; Zhu, L.; Al-Kaysi, R. O.; Bardeen, C. J. Organic Photomechanical Materials. *ChemPhysChem* **2014**, *15*, 400–414.

(7) Naumov, P.; Chizhik, S.; Panda, M. K.; Nath, N. K.; Boldyreva, E. Mechanically Responsive Molecular Crystals. *Chem. Rev.* **2015**, *115*, 12440–12490.

(8) Yu, Q.; Aguila, B.; Gao, J.; Xu, P.; Chen, Q.; Yan, J.; Xing, D.; Chen, Y.; Cheng, P.; Zhang, Z. et al. Photomechanical Organic Crystals as Smart Materials for Advanced Applications. *Chem. Eur. J.* **2019**, *25*, 5611–5622.

(9) Naumov, P.; Karothu, D. P.; Ahmed, E.; Catalano, L.; Commins, P.; Mahmoud Halabi, J.; Al-Handawi, M. B.; Li, L. The Rise of the Dynamic Crystals. *J. Am. Chem. Soc.* **2020**, *142*, 13256–13272.

(10) Huang, C.; Huang, R.; Zhang, S.; Sun, H.; Wang, H.; Du, B.; Xiao, Y.; Yu, T.; Huang, W. Recent Development of Photodeformable Crystals: From Materials to Mechanisms. *Research* **2021**, *2021*, 9816535.

(11) Karothu, D. P.; Mahmoud Halabi, J.; Li, L.; Colin-Molina, A.; Rodríguez-Molina, B.; Naumov, P. Global Performance Indices for Dynamic Crystals as Organic Thermal Actuators. *Adv. Mater.* **2020**, *32*, 1906216.

(12) Mahmoud Halabi, J.; Ahmed, E.; Sofela, S.; Naumov, P. Performance of Molecular Crystals in Conversion of Light to Mechanical Work. *Proc. Nat. Acad. Sci.* **2021**, *118*, 1–7.

(13) Karothu, D. P.; Mahmoud Halabi, J.; Ahmed, E.; Ferreira, R.; Spackman, P. R.; Spackman, M. A.; Naumov, P. Global Analysis of the Mechanical Properties of Organic Crystals. *Angew. Chem. Int. Ed.* **2022**, *61*, e202113988.

(14) Taniguchi, T.; Asahi, T.; Koshima, H. Photomechanical Azobenzene Crystals. *Crystals* **2019**, *9*, 437.

(15) Koshima, H.; Takechi, K.; Uchimoto, H.; Shiro, M.; Hashizume, D. Photomechanical Bending of Salicylideneaniline Crystals. *Chem. Commun.* **2011**, *47*, 11423.

(16) Hasebe, S.; Hagiwara, Y.; Takechi, K.; Katayama, T.; Furube, A.; Asahi, T.; Koshima, H. Polymorph-Derived Diversification of Crystal Actuation by Photoisomerization and the Photothermal Effect. *Chem. Mater.* **2022**, *34*, 1315–1324.

(17) Kobatake, S.; Takami, S.; Muto, H.; Ishikawa, T.; Irie, M. Rapid and Reversible Shape Changes of Molecular Crystals on Photoirradiation. *Nature* **2007**, *446*, 778–781.

(18) Colombier, I.; Spagnoli, S.; Corval, A.; Baldeck, P. L.; Giraud, M.; Leaustic, A.; Yu, P.; Irie, M. Diarylethene Microcrystals Make Directional Jumps Upon Ultraviolet Irradiation. *J. Chem. Phys.* **2007**, *126*, 011101.

(19) Uchida, K.; Sukata, S.-i.; Matsuzawa, Y.; Akazawa, M.; de Jong, J. J. D.; Katsonis, N.; Kojima, Y.; Nakamura, S.; Areephong, J.; Meetsma, A. et al. Photoresponsive Rolling and Bending of Thin Crystals of Chiral Diarylethenes. *Chem. Commun.* **2008**, 326–328.

(20) Morimoto, M.; Irie, M. A Diarylethene Cocrystal that Converts Light into Mechanical Work. *J. Am. Chem. Soc.* **2010**, *132*, 14172–14178.

(21) Terao, F.; Morimoto, M.; Irie, M. Light-Driven Molecular-Crystal Actuators: Rapid and Reversible Bending of Rodlike Mixed Crystals of Diarylethene Derivatives. *Angew. Chem. Int. Ed.* **2012**, *51*, 901–904.

(22) Kitagawa, D.; Nishi, H.; Kobatake, S. Photoinduced Twisting of a Photochromic Diarylethene Crystal. *Angew. Chem. Int. Ed.* **2013**, *52*, 9320–9322.

(23) Ohshima, S.; Morimoto, M.; Irie, M. Light-Driven Bending of Diarylethene Mixed Crystals. *Chem. Sci.* **2015**, *6*, 5746–5752.

(24) Tong, F.; Kitagawa, D.; Dong, X.; Kobatake, S.; Bardeen, C. J. Photomechanical Motion of Diarylethene Molecular Crystal Nanowires. *Nanoscale* **2018**, *10*, 3393–3398.

(25) Fujimoto, A.; Fujinaga, N.; Nishimura, R.; Hatano, E.; Kono, L.; Nagai, A.; Sekine, A.; Hattori, Y.; Kojima, Y.; Yasuda, N. et al. Photoinduced Swing of a Diarylethene Thin Broad Sword-Shaped Crystal: A Study on the Detailed Mechanism. *Chem. Sci.* **2020**, *11*, 12307–12315.

(26) Irie, M.; Fukaminato, T.; Matsuda, K.; Kobatake, S. Photochromism of Diarylethene Molecules and Crystals: Memories, Switches, and Actuators. *Chem. Rev.* **2014**, *114*, 12174–12277.

(27) Sun, J.-K.; Li, W.; Chen, C.; Ren, C.-X.; Pan, D.-M.; Zhang, J. Photoinduced Bending of a Large Single Crystal of a 1,2-Bis(4-pyridyl)ethylene-Based Pyridinium Salt Powered by a [2+2] Cycloaddition. *Angew. Chem. Int. Ed.* **2013**, *52*, 6653–6657.

(28) Medishetty, R.; Husain, A.; Bai, Z.; Runčevski, T.; Dinnebier, R. E.; Naumov, P.; Vittal, J. J. Single Crystals Popping Under UV Light: A Photosalient Effect Triggered by a [2+2] Cycloaddition Reaction. *Angew. Chem. Int. Ed.* **2014**, *53*, 5907–5911.

(29) Nath, N. K.; Runčevski, T.; Lai, C.-Y.; Chiesa, M.; Dinnebier, R. E.; Naumov, P. Surface and Bulk Effects in Photochemical Reactions and Photomechanical Effects in Dynamic Molecular Crystals. *J. Am. Chem. Soc.* **2015**, *137*, 13866–13875.

(30) Wang, H.; Chen, P.; Wu, Z.; Zhao, J.; Sun, J.; Lu, R. Bending, Curling, Rolling, and Salient Behavior of Molecular Crystals Driven by [2+2] Cycloaddition of a Styrylbenzoxazole Derivative. *Angew. Chem. Int. Ed.* **2017**, *56*, 9463–9467.

(31) Al-Kaysi, R. O.; Müller, A. M.; Bardeen, C. J. Photochemically Driven Shape Changes of Crystalline Organic Nanorods. *J. Am. Chem. Soc.* **2006**, *128*, 15938–15939.

(32) Zhu, L.; Al-Kaysi, R. O.; Bardeen, C. J. Reversible Photoinduced Twisting of Molecular Crystal Microribbons. *J. Am. Chem. Soc.* **2011**, *133*, 12569–12575.

(33) Jezowski, S. R.; Zhu, L.; Wang, Y.; Rice, A. P.; Scott, G. W.; Bardeen, C. J.; Chronister, E. L. Pressure Catalyzed Bond Dissociation in an Anthracene Cyclophane Photodimer. *J. Am. Chem. Soc.* **2012**, *134*, 7459–7466.

(34) Kim, T.; Al-Muhanna, M. K.; Al-Suwaidan, S. D.; Al-Kaysi, R. O.; Bardeen, C. J. Photoinduced Curling of Organic Molecular Crystal Nanowires. *Angew. Chem. Int. Ed.* **2013**, *52*, 6889–6893.

(35) Dong, X.; Tong, F.; Hanson, K. M.; Al-Kaysi, R. O.; Kitagawa, D.; Kobatake, S.; Bardeen, C. J. Hybrid Organic–Inorganic Photon-Powered Actuators Based on Aligned Diarylethene

Nanocrystals. *Chem. Mater.* **2019**, *31*, 1016–1022.

(36) Tong, F.; Xu, W.; Guo, T.; Lui, B. F.; Hayward, R. C.; Palffy-Muhoray, P.; Al-Kaysi, R. O.; Bardeen, C. J. Photomechanical Molecular Crystals and Nanowire Assemblies Based on the [2+2] Photodimerization of a Phenylbutadiene Derivative. *J. Mater. Chem. C* **2020**, *8*, 5036–5044.

(37) Uchida, E.; Azumi, R.; Norikane, Y. Light-Induced Crawling of Crystals on a Glass Surface. *Nature Commun.* **2015**, *6*, 7310.

(38) Tong, F.; Kitagawa, D.; Bushnak, I.; Al-Kaysi, R. O.; Bardeen, C. J.; Al-Kaysi, R. O.; Bardeen, C. J. Light-Powered Autonomous Flagella-Like Motion of Molecular Crystal Microwires. *Angew. Chem. Int. Ed.* **2021**, *60*, 2414–2423.

(39) Venkatakrishnarao, D.; Mohiddon, M. A.; Chandrasekhar, N.; Chandrasekar, R. Photonic Microrods Composed of Photoswitchable Molecules: Erasable Heterostructure Waveguides for Tunable Optical Modulation. *Adv. Opt. Mater.* **2015**, *3*, 1035–1040.

(40) Halabi, J. M.; Ahmed, E.; Catalano, L.; Karothu, D. P.; Rezgui, R.; Naumov, P. Spatial Photocontrol of the Optical Output from an Organic Crystal Waveguide. *J. Am. Chem. Soc.* **2019**, *141*, 14966–14970.

(41) Morimoto, M.; Kobatake, S.; Irie, M. Polymorphism of 1,2-Bis(2-methyl-5-p-methoxyphenyl-3-thienyl)perfluorocyclopentene and Photochromic Reactivity of the Single Crystals. *Chem. Eur. J.* **2003**, *9*, 621–627.

(42) Salzillo, T.; Brillante, A. Commenting on the Photoreactions of Anthracene Derivatives in the Solid State. *CrystEngComm* **2019**, *21*, 3127–3136.

(43) Lan, L.; Di, Q.; Li, L.; Liu, B.; Yu, X.; Naumov, P.; Zhang, H. Packing-Dependent Mechanical Properties of Schiff Base Crystals. *Cryst. Growth Des.* **2022**, *22*, 3435–3441.

(44) Gately, T. J.; Cook, C. C.; Almuzarie, R.; Islam, I.; Gardner, Z. T.; Iuliucci, R. J.; Al-Kaysi, R. O.; Beran, G. J. O.; Bardeen, C. J. Effect of Fluorination on Polymorphism and the Photomechanical Performance of Cinnamalmalonitrile Crystals. *Cryst. Growth Des.* **2022**, *22*, 7298–7307.

(45) Gately, T. J.; Sontising, W.; Easley, C. J.; Islam, I.; Al-Kaysi, R. O.; Beran, G. J. O.; Bardeen, C. J. Effect of Halogen Substitution on Energies and Dynamics of Reversible Photomechanical Crystals Based on 9-Anthracenecarboxylic Acid. *CrystEngComm* **2021**, *23*, 5931–5943.

(46) Cook, C. J.; Li, W.; Lui, B. F.; Gately, T. J.; Al-Kaysi, R. O.; Mueller, L. J.; Bardeen, C. J.; Beran, G. J. O. A Theoretical Framework for the Design of Photomechanical Engines. *Chem. Sci.* **2022**, *14*, 937–949.

(47) Kobatake, S.; Yamada, T.; Uchida, K.; Kato, N.; Irie, M. Photochromism of 1,2-Bis(2,5-dimethyl-3-thienyl)perfluorocyclopentene in a Single Crystalline Phase. *J. Am. Chem. Soc.* **1999**, *121*, 2380–2386.

(48) Yamada, T.; Kobatake, S.; Irie, M. X-Ray Crystallographic Study on Single-Crystalline Photochromism of 1,2-Bis(2,5-dimethyl-3-thienyl)perfluorocyclopentene. *Bull. Chem. Soc. Jpn.* **2000**, *73*, 2179–2184.

(49) Yamada, T.; Kobatake, S.; Muto, K.; Irie, M. X-ray Crystallographic Study on Single-Crystalline Photochromism of Bis(2,5-dimethyl-3-thienyl)perfluorocyclopentene. *J. Am. Chem. Soc.* **2000**, *122*, 1589–1592.

(50) Morimoto, M.; Kobatake, S.; Irie, M. Multicolor Photochromism of Two- and Three-Component Diarylethene Crystals. *J. Am. Chem. Soc.* **2003**, *125*, 11080–11087.

(51) Morimoto, M.; Irie, M. Photochromism of Diarylethene Single Crystals: Crystal Structures and Photochromic Performance. *Chem. Commun.* **2005**, 3895–3905.

(52) Kuroki, L.; Takami, S.; Yoza, K.; Morimoto, M.; Irie, M. Photoinduced Shape Changes of Diarylethene Single Crystals: Correlation Between Shape Changes and Molecular Packing. *Photochem. Photobio. Sci.* **2010**, *9*, 221–225.

(53) Nakamura, S.; Irie, M. Thermally Irreversible Photochromic Systems. A Theoretical Study. *J. Org. Chem.* **1988**, *53*, 6136–6138.

(54) Turowska-Tyrk, I.; Trzop, E. Monitoring Structural Transformations in Crystals. 6. The [4 + 4] Photodimerization of 9-Methyl-Anthracene. *Acta Cryst. B* **2003**, *59*, 779–786.

(55) Bąkowicz, J.; Turowska-Tyrk, I. The Role of Free Space in Photochemical Reactions in Crystals at High Pressure—The Case of 9-Methylanthracene. *Acta Cryst. B* **2022**, *78*, 223–230.

(56) Yang, C.; Zhu, L.; Kudla, R. A.; Hartman, J. D.; Al-Kaysi, R. O.; Monaco, S.; Schatschneider, B.; Magalhaes, A.; Beran, G. J. O.; Bardeen, C. J. et al. Crystal Structure of The Meta-Stable Intermediate in the Photomechanical, Crystal-to-Crystal Reaction of 9-tertbutyl Anthracene Ester. *CrystEngComm* **2016**, *18*, 7319–7329.

(57) Chalek, K. R.; Dong, X.; Tong, F.; Kudla, R. A.; Zhu, L.; Gill, A. D.; Xu, W.; Yan, C.; Hartman, J. D.; Magalhaes, A. et al. Bridging Photochemistry and Photomechanics with NMR crystallography: The Molecular Basis for the Macroscopic Expansion of an Anthracene Ester Nanorod. *Chem. Sci.* **2021**, *12*, 453–463.

(58) Al-Kaysi, R. O.; Bardeen, C. J. Reversible Photoinduced Shape Changes of Crystalline Organic Nanorods. *Adv. Mater.* **2007**, *19*, 1276–1280.

(59) Takanabe, A.; Tanaka, M.; Johmoto, K.; Uekusa, H.; Mori, T.; Koshima, H.; Asahi, T. Optical Activity and Optical Anisotropy in Photomechanical Crystals of Chiral Salicylidenephenylethylamines. *J. Am. Chem. Soc.* **2016**, *138*, 15066–15077.

(60) Li, P.; Guan, J.; Peng, M.; Wu, J.; Yin, M. Spontaneous and Photomechanical Twisting of a Cyanostilbene-based Molecular Crystal. *J. Mater. Chem. C* **2023**,

(61) Giannozzi, P.; Andreussi, O.; Brumme, T.; Bunau, O.; Buongiorno Nardelli, M.; Calandra, M.; Car, R.; Cavazzoni, C.; Ceresoli, D.; Cococcioni, M. et al. Advanced Capabilities for Materials Modelling with Quantum ESPRESSO. *J. Phys. Condens. Mat.* **2017**, *29*, 465901.

(62) Becke, A. D. On the Large-Gradient Behavior of the Density Functional Exchange Energy. *J. Chem. Phys.* **1986**, *85*, 7184–7187.

(63) Perdew, J. P.; Burke, K.; Ernzerhof, M. Generalized Gradient Approximation Made Simple. *Phys. Rev. Lett.* **1996**, *77*, 3865.

(64) Otero-de-la Roza, A.; Johnson, E. R. Van der Waals Interactions in Solids Using the Exchange-Hole Dipole Moment Model. *J. Chem. Phys.* **2012**, *136*, 174109.

(65) Chisholm, J. A.; Motherwell, W. D. S. COMPACK: A Program for Identifying Crystal Structure Similarity Using Distances. *J. Appl. Crystall.* **2005**, *38*, 228–231.

(66) Beran, G. J. O. First-Principles Computations Indicate that Solid State Photodimerization of 9-*tert*-butyl Anthracene Ester Produces an Exceptionally Metastable Polymorph. *CrystEngComm* **2019**, *21*, 758–764.

(67) Kobatake, S.; Morimoto, M.; Asano, Y.; Murakami, A.; Nakamura, S.; Irie, M.; Ã, M. I.; Irie, M. Absorption Spectra of Colored Isomer of Diarylethene in Single Crystals. *Chem. Lett.* **2002**, *31*, 1224–1225.

(68) Karothu, D. P.; Ferreira, R.; Dushaq, G.; Ahmed, E.; Catalano, L.; Halabi, J. M.; Alhaddad, Z.; Tahir, I.; Li, L.; Mohamed, S. et al. Exceptionally High Work Density of a Ferroelectric Dynamic Organic Crystal Around Room Temperature. *Nature Commun.* **2022**, *13*, 2823.

(69) Xu, T.-Y.; Tong, F.; Xu, H.; Wang, M.-Q.; Tian, H.; Qu, D.-H. Engineering Photomechanical Molecular Crystals to Achieve Extraordinary Expansion Based on Solid-State [2 + 2] Photocycloaddition. *J. Am. Chem. Soc.* **2022**, *144*, 6278–6290.

(70) Woodcock, H. L.; Schaefer, H. F.; Schreiner, P. R. Problematic Energy Differences Between Cumulenes and Polyynes: Does This Point to a Systematic Improvement of Density Functional Theory? *J. Phys. Chem. A* **2002**, *106*, 11923–11931.

(71) Heaton-Burgess, T.; Yang, W. Structural Manifestation of the Delocalization Error of Density Functional Approximations: C4N+2 Rings and C_{20} Bowl, Cage, and Ring Isomers. *J. Chem. Phys.* **2010**, *132*, 234113.

(72) Whittleton, S. R.; Otero-de-la Roza, A.; Johnson, E. R. Exchange-Hole Dipole Dispersion Model for Accurate Energy Ranking in Molecular Crystal Structure Prediction II: Nonplanar Molecules. *J. Chem. Theory Comput.* **2017**, *13*, 5332–5342.

(73) Greenwell, C.; McKinley, J. L.; Zhang, P.; Zeng, Q.; Sun, G.; Li, B.; Wen, S.; Beran, G. J. O. Overcoming the Difficulties of Predicting Conformational Polymorph Energetics in Molecular Crystals Via Correlated Wavefunction Methods. *Chem. Sci.* **2020**, *11*, 2200–2214.

(74) Greenwell, C.; Beran, G. J. O. Inaccurate Conformational Energies Still Hinder Crystal Structure Prediction in Flexible Organic Molecules. *Cryst. Growth Des.* **2020**, *20*, 4875–4881.

(75) Greenwell, C.; Beran, G. J. O. Rubrene Untwisted: Common Density Functional Theory Calculations Overestimate Its Deviant Tendencies. *J. Mater. Chem. C* **2021**, *9*, 2848–2857.

(76) Beran, G. J. O.; Sugden, I. J.; Greenwell, C.; Bowskill, D. H.; Pantelides, C. C.; Adjiman, C. S. How Many More Polymorphs of ROY Remain Undiscovered? *Chem. Sci.* **2022**, *13*, 1288–1297.

(77) Beran, G. J. O.; Wright, S. E.; Greenwell, C.; Cruz-Cabeza, A. J. The Interplay of Intra- and Intermolecular Errors in Modeling Conformational Polymorphs. *J. Chem. Phys.* **2022**, *156*, 104112.

(78) Guo, Y.; Riplinger, C.; Becker, U.; Liakos, D. G.; Minenkov, Y.; Cavallo, L.; Neese, F. Communication: An improved linear scaling perturbative triples correction for the domain based local pair-natural orbital based singles and doubles coupled cluster method [DLPNO-CCSD(T)]. *J. Chem. Phys.* **2018**, *148*, 011101.

(79) Neese, F. The ORCA program system. *WIREs Comput. Molec. Sci.* **2012**, *2*, 73–78.

(80) Nyman, J.; Day, G. M. Static and Lattice Vibrational Energy Differences Between Polymorphs. *CrystEngComm* **2015**, *17*, 5154–5165.

(81) Cruz-Cabeza, A. J.; Reutzel-Edens, S. M.; Bernstein, J. Facts and Fictions About Polymorphism. *Chem. Soc. Rev.* **2015**, *44*, 8619–8635.

(82) Ware, T. H.; McConney, M. E.; Wie, J. J.; Tondiglia, V. P.; White, T. J. Voxelated Liquid Crystal Elastomers. *Science* **2015**, *347*, 982–984.

(83) Helgaker, T.; Klopper, W.; Koch, H.; Noga, J. Basis-Set Convergence of Correlated Calculations on Water. *J. Chem. Phys.* **1997**, *106*, 9639–9646.

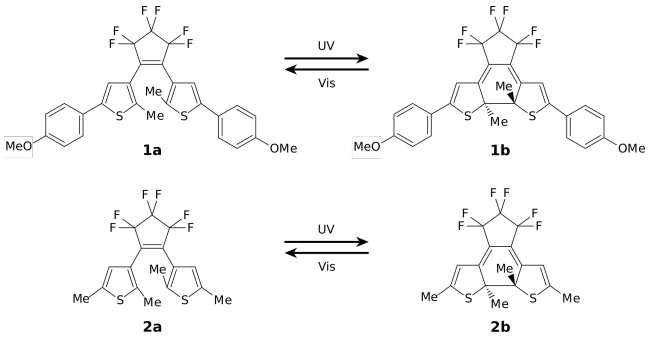

Figure 1: Photochromic reactions of 1,2-bis(2-methyl-5-p-methoxyphenyl-3-thienyl)perfluoro-cyclopentene (**1**) and bis(2,5-dimethyl-3-thienyl)perfluoro-cyclopentene (**2**).

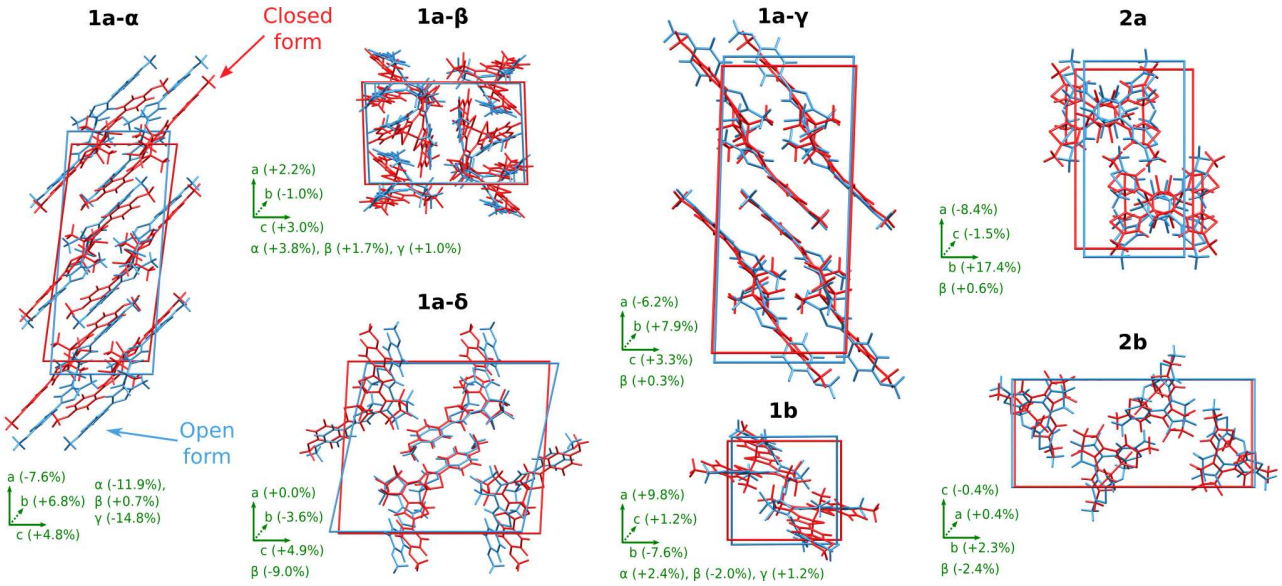

Figure 2: Crystal structure overlays showing the predicted solid-state transformations of seven crystal forms of **1** and **2**. Crystallographic orientations and percent changes in the lattice parameters for the forward-direction reactions are indicated in green.

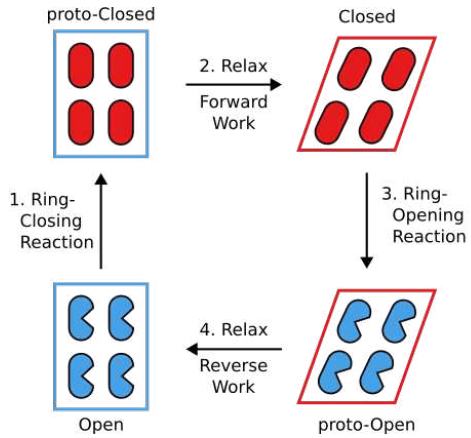

Figure 3: Schematic photomechanical engine cycle starting from open-ring diarylethene crystals of **1a** or **2a**. Steps 1 & 3 involve chemical reactions in a fixed unit cell, thereby generating stress and strain. Subsequent complete crystal structure relaxation in Steps 2 & 4 performs the forward and reverse work, respectively. For closed-form **1b** and **2b**, the engine cycle begins with ring-opening.

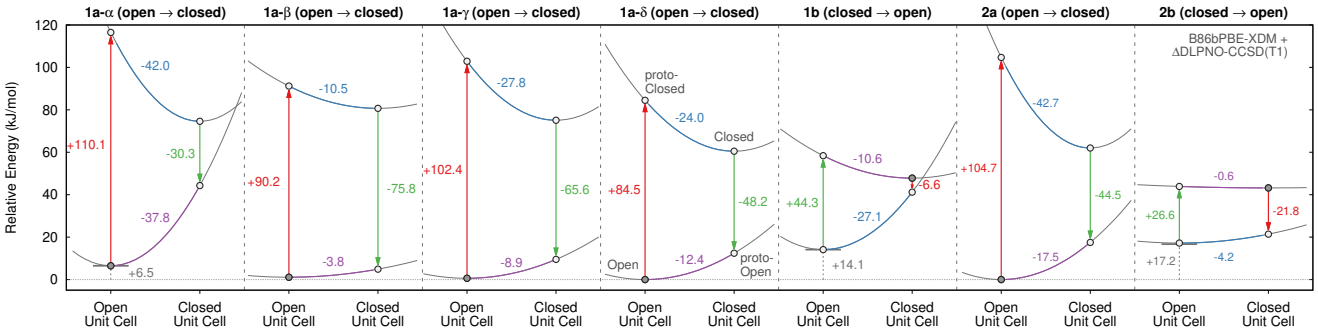

Figure 4: Predicted photomechanical engine cycles for the crystal forms of **1** and **2**, with Steps 1-4 in red, blue, green, and purple, respectively. The numbers indicate the energy change for each step in kJ/mol. The dark gray circle indicates the starting structure of each. Energies are reported relative to the most stable crystal forms (**1a-**γ or **2a**).

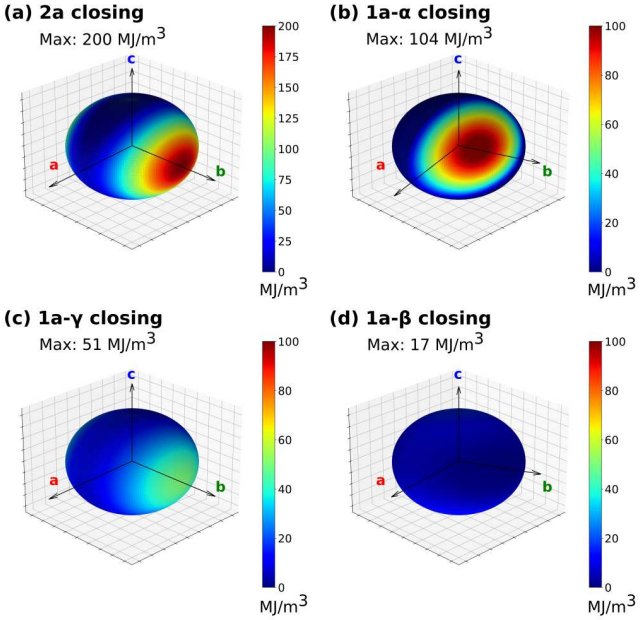

Figure 5: Anisotropic work density plots for the forward-direction closing reactions of (a) **2a**, (b) **1a-**α, (c) **1a-**γ, and (d) **1a-**β. The heat map indicates the work density (in MJ/m^3) along different crystallographic directions. Note the heat map scale for (a) differs from (b)–(d). The first three exhibit large maximum work densities along high stress and strain directions, while the **1a-**β transforms more isotropically and exhibits much smaller work densities. See SI Section S2.2 for the complete set of work density plots.